

## X-RAY PROPERTIES OF THE WEAK SEYFERT 1 NUCLEUS IN NGC 4639

LUIS C. HO

Carnegie Observatories, 813 Santa Barbara Street, Pasadena, CA 91101-1292

ANDREW PTAK

Department of Physics, Carnegie Mellon University, Pittsburgh, PA 15213

YUICHI TERASHIMA

NASA/GSFC, Code 662, Greenbelt, MD 20771

HIDEYO KUNIEDA

Department of Astrophysics, Nagoya University, Chikusa-ku, Nagoya 464-01, Japan

PETER J. SERLEMITSOS AND TAHIR YAQOUB

NASA/GSFC, Code 662, Greenbelt, MD 20771

AND

ANURADHA P. KORATKAR

Space Telescope Science Institute, 3700 San Martin Drive, Baltimore, MD 21218

Received 1999 March 31; accepted 1999 June 22

### ABSTRACT

Low-luminosity active galactic nuclei (AGNs), of which NGC 4639 is a good example, constitute an important but poorly understood constituent of the nearby galaxy population. We obtained observations of NGC 4639 with *ASCA* in order to investigate its mildly active Seyfert 1 nucleus at hard X-ray energies. Koratkar et al. have previously shown that the nucleus is a pointlike source in the *ROSAT* soft X-ray band. We detected in the 2–10 keV band a compact central source with a luminosity of  $8.3 \times 10^{40}$  ergs  $s^{-1}$  (for an adopted distance of 25.1 Mpc). Comparison of the *ASCA* data with archival data taken with the *Einstein* and *ROSAT* satellites shows that the nucleus varies on timescales of months to years. The variability could be intrinsic, or it could be caused by variable absorption. More rapid variability, on a timescale of  $\sim 10^4$  s, may be present in the *ASCA* data. The spectrum from 0.5 to 10 keV is well described by a model consisting of a lightly absorbed ( $N_H = 7.3 \times 10^{20}$   $cm^{-2}$ ) power law with a photon index of  $\Gamma = 1.68 \pm 0.12$ . We find no evidence for significant emission from a thermal plasma; if present, it can account for no more than  $\sim 25\%$  of the flux in the 0.5–2.0 keV band. The limited photon statistics of our data do not allow us to place significant limits on the presence of iron K emission. Despite its low luminosity, the X-ray properties of the nucleus of NGC 4639 appear quite normal compared with those of more luminous AGNs. The strength of its broad  $H\alpha$  line follows the correlation between broad  $H\alpha$  luminosity and hard X-ray luminosity that was previously known for luminous objects. Images taken with the *Hubble Space Telescope* detected the nucleus in the ultraviolet at a strength relative to the X-ray band that appears to be quite typical of that found in other AGNs. NGC 5033, another low-luminosity Seyfert 1 galaxy with optical characteristics that closely resemble those of NGC 4639, has also been studied recently with *ASCA*, and we highlight some of the similarities between these two objects.

*Subject headings:* galaxies: active — galaxies: individual (NGC 4639) — galaxies: nuclei — galaxies: Seyfert — X-rays: galaxies

### 1. BACKGROUND

NGC 4639 is one of the weakest known Seyfert galaxies. Its active nucleus was discovered by Filippenko & Sargent (1986) during the course of an extensive optical spectroscopic survey of nearby galaxies (Filippenko & Sargent 1985; Ho, Filippenko, & Sargent 1995). NGC 4639 is a moderately inclined, bulge-dominated barred spiral; Sandage & Tammann (1981) assign it a Hubble type of SBb, and de Vaucouleurs et al. (1991) favor a classification of SABbc. The Cepheid-based distance of the galaxy has been determined by Sandage et al. (1996) to be 25.1 Mpc. The optical spectrum of the nucleus exhibits prominent hydrogen Balmer emission lines with velocities of  $\sim 4000$   $km\ s^{-1}$  at FWHM. According to the criteria of Osterbrock (1981), the relative strengths of the broad Balmer lines formally qualify the nucleus as a Seyfert of type 1.0 (Ho et al. 1997b). By traditional standards, however, the nucleus of NGC 4639 is intrinsically quite weak. Ho et al. (1997b) measure a

luminosity of  $\sim 1 \times 10^{40}$  ergs  $s^{-1}$  for the broad  $H\alpha$  emission line. The pointlike nucleus, while visible in *Hubble Space Telescope* (*HST*) images taken at optical wavelengths (Calvani et al. 1999), is nonetheless rather faint:  $B \approx 19.5$  mag, or  $M_B \approx -12.5$  mag—at least a factor of  $10^4$  fainter than the most luminous Seyfert nuclei ( $M_B \approx -23$  mag; Weedman 1976).

Very little information exists for active galactic nuclei (AGNs) in the luminosity regime of NGC 4639. Detailed studies of such objects are not only of intrinsic interest, but, by exploring new parameter space, may illuminate our understanding of the AGN phenomenon in general. The data deficiency is particularly acute at X-ray energies, where poor angular resolution and low sensitivity have been major hindrances in detecting and isolating a faint nucleus from the surrounding light of the host galaxy. Substantial progress has been made in the past few years with the advent of *ROSAT* and *ASCA* (see, e.g., Koratkar et al. 1995;

Ishizaki et al. 1996; Serlemitsos, Ptak, & Yaqoob 1996; Iyomoto et al. 1998; Nicholson et al. 1998; Ptak et al. 1999; Terashima 1999), but the samples studied so far remain very small and are largely biased against low-luminosity Seyferts.

Here we present new X-ray observations of NGC 4639 obtained with *ASCA*. We will combine these observations with existing data taken with *ROSAT* and with *HST* in order to derive a more complete picture of the X-ray properties of the source.

## 2. X-RAY OBSERVATIONS

The *ASCA* data were acquired on 1997 December 17 and 23 UT; a description of the satellite can be found in Tanaka, Inoue, & Holt (1994). *ASCA* consists of four identical X-ray telescopes whose focal plane is equipped with two solid-state imaging spectrometers (SIS0 and SIS1) and two gas-imaging spectrometers (GIS2 and GIS3). The SIS covers the energy range 0.6–10.0 keV with a resolution (FWHM) of  $E/\Delta E \approx 50$  at 6 keV and  $\sim 20$  at 1.5 keV; each camera has a field of view of approximately  $22' \times 22'$ , although in these observations only one CCD was active, resulting in a field of view of  $\sim 11' \times 11'$ . The GIS has lower spectral resolution than the SIS ( $E/\Delta E \approx 13$  at 6 keV and  $\sim 7$  at 1.5 keV), but it has higher efficiency in the hard X-rays over the bandpass 0.7–10.0 keV; the usable field of view of the GIS has a circular diameter  $\sim 40'$ . The point-spread function (PSF) of the images has a half-power diameter of  $3'$ , with  $\sim 20\%$  of the photons concentrated in a sharp core of diameter  $1'$ . In practice, the SIS delivers images of higher angular resolution than the GIS, whose PSF core is somewhat adversely affected by errors from position determination.

We operated the SIS in the 1-CCD faint mode, and the GIS was used in the nominal pulse-height mode. We screened the data using standard criteria, which include the exclusion of data taken when the elevation angle was less than  $25^\circ$  for SIS and less than  $5^\circ$  for GIS, when the geomagnetic cutoff rigidity was less than  $6 \text{ GeV } c^{-1}$ , and during passage through the South Atlantic Anomaly. So-called hot and flickering pixels were also removed from the SIS data. The final integration times for the SIS and GIS data sets are 66.8 ks and 71.1 ks, respectively. The light curves and spectra, discussed in the next section, were extracted using a circular aperture of radius  $4'$  for the SIS and  $6'$  for the GIS. We measured the background from a source-free region within the same field. After background subtraction, the count rates for SIS0, SIS1, GIS2, and GIS3, averaged over the two observations, are 0.034, 0.033, 0.019, and 0.021 counts  $s^{-1}$ , respectively. We combined the SIS0 and SIS1 spectra after appropriate gain corrections and similarly for the GIS2 and GIS3 spectra. To permit  $\chi^2$  analysis, the spectra were binned such that each bin contains at least 20 counts.

## 3. ANALYSIS

### 3.1. Spatial Fitting

Figure 1 displays the SIS0 + SIS1 contour image of NGC 4639 taken on 1997 December 17, superposed on an optical image of the galaxy taken from the Digital Sky Survey. A compact source positionally coincides with the optical nucleus. In order to analyze the spatial extent of X-ray data properly, particularly in the case of *ASCA*, the contribution of the PSF must be taken into account. In

order to do this, we produced a model PSF and then convolved it with a model consisting of a single Gaussian,  $S(r) = N \exp[-(r^2/2\sigma^2)]$ , or a double Gaussian,  $S(r) = N_1 \exp[-(r^2/2\sigma_1^2)] + N_2 \exp[-(r^2/2\sigma_2^2)]$ . The best-fit spectral model for the *ASCA* data (§ 3.2) was used to simulate the energy dependence of the PSF. We analyzed only the SIS0 data from the first observation; combining data from both SIS detectors for spatial analysis is problematic, because the source lies at different off-axis angles in the two detectors. We find that a single Gaussian provides an acceptable fit: the source is consistent with being unresolved, with an upper limit size of  $\sigma \approx 30''$ .

We have also reanalyzed the *ROSAT* high-resolution imager (HRI) image of NGC 4639 previously published by Koratkar et al. (1995), and we adopt an analytic formula<sup>1</sup> as a model of the HRI PSF. The HRI data were split into two observations separated by  $\sim 5$  months. The latter observation is consistent with a single Gaussian fit with  $\sigma \approx 2''$ . In addition to the dominant compact source, the earlier of the two observations shows measurable excess emission at  $\sim 25''$ , at a level of  $\sim 2\%$  of the total count rate. This extra component may be due to a variable source, such as a background quasar, although inspection of the two images does not reveal any obvious point source apart from the galaxy nucleus. Alternatively, the low-level emission may be an artifact of PSF variations, which have been known to occur at this level (E. Colbert 1999, private communication). Given that NGC 4639 does show evidence of long-term variability (§ 3.3), it is reasonable to assume that essentially all of the X-ray flux from NGC 4639 is unresolved, with a half-light radius on the order of  $2''$  ( $\sim 240 \text{ pc}$ ) or less.

### 3.2. Spectral Fitting

After reducing the *ASCA* data, we extracted separate spectra for each of the SIS and GIS detectors, resulting in a set of eight source and eight background spectra for the two observations. We find that the SIS0 and SIS1 spectra are consistent with each other, as are the GIS2 and GIS3 spectra, and, accordingly, the data from each detector were combined. (SIS and GIS spectra cannot be combined because the detectors have different bandpasses and responses.) This resulted in two SIS and two GIS spectra. In the following, we fit the four spectra simultaneously, leaving the overall normalization to be a free parameter (to allow for systematic uncertainty in the flux calibration of each set of detectors and for variability between the two observations). A model consisting of a power law modified by photoelectric absorption provides an acceptable fit to all four spectra (the reduced  $\chi^2$ ,  $\chi^2_\nu$ , is 0.98 for 491 dof), resulting in a column density of  $N_{\text{H}} = 7.3 (2.2\text{--}12.9) \times 10^{20} \text{ cm}^{-2}$  and a photon index of  $\Gamma = 1.68 (1.56\text{--}1.80)$ , where the values in parentheses give the 90% confidence interval assuming two interesting parameters. For comparison, the foreground absorbing column due to the Galaxy is  $N_{\text{H}} = 2.3 \times 10^{20} \text{ cm}^{-2}$  (Murphy et al. 1996), and, for an assumed case B' ratio  $H\alpha/H\beta = 3.1$  (see Gaskell & Ferland 1984), the decrement of the narrow Balmer lines measured by Ho, Filippenko, & Sargent (1997a) indicates an internal reddening of  $E(B-V) \approx 0.03 \text{ mag}$ , which corresponds to  $N_{\text{H}} \approx 2 \times 10^{20} \text{ cm}^{-2}$  for the conversion  $E(B-V) = N_{\text{H}}/(5.8$

<sup>1</sup> This formula is given in [http://heasarc.gsfc.nasa.gov/docs/rosat/faqs/hri\\_psf\\_faq1.html](http://heasarc.gsfc.nasa.gov/docs/rosat/faqs/hri_psf_faq1.html).

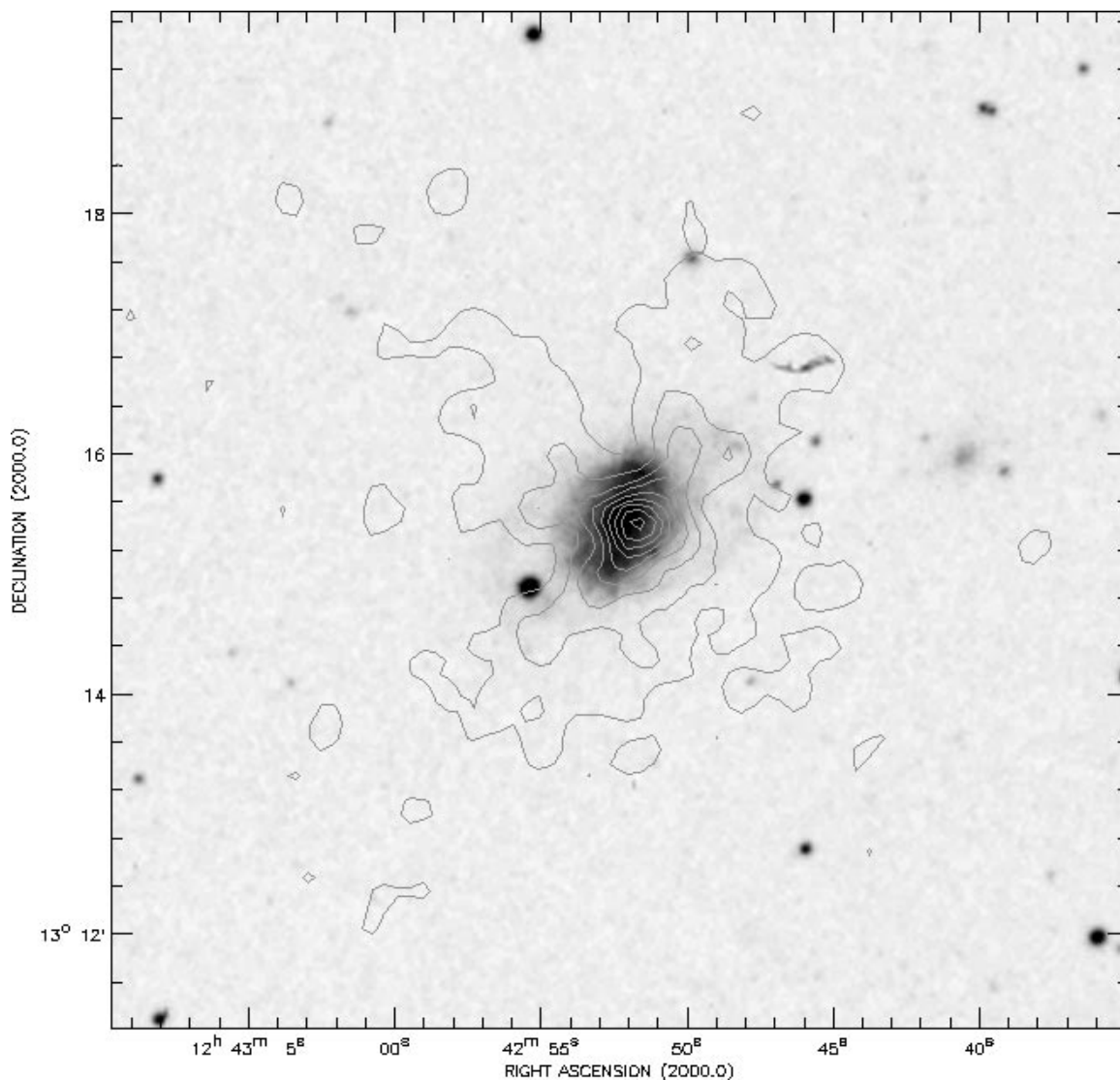


FIG. 1.—*ASCA* SIS0 + SIS1 contour image of NGC 4639 superposed on an optical image of the galaxy taken from the Digital Sky Survey. For the purposes of the display, the *ASCA* image has been smoothed with a Gaussian of width 6". The contour levels are linear, and they begin at  $1.6 \times 10^{-5}$  counts  $s^{-1}$ .

$\times 10^{21}$   $cm^{-2}$ ) mag (Bohlin, Savage, & Drake 1978). The spectra, their fits, and the residuals of the fits are shown in Figure 2. The observed 2–10 keV flux is  $1.1 \times 10^{-12}$  ergs  $s^{-1}$   $cm^{-2}$  (corresponding to a luminosity of  $8.3 \times 10^{40}$  ergs  $s^{-1}$  for an adopted distance of 25.1 Mpc) for all but the second SIS observation, which gave a flux  $\sim 25\%$  higher. *ASCA* fluxes typically have uncertainties of  $\sim 10\%$ – $20\%$ , so the flux discrepancy of the second observation is somewhat large but probably not inconsistent with the calibration uncertainty of the detectors.

Previous *ASCA* observations have shown that low-luminosity AGNs typically emit a soft, thermal component in their X-ray spectra (e.g., Serlemitsos et al. 1996; Ptak et al. 1999), and it would be of interest to see if NGC 4639 follows this pattern. We attempted to fit the spectra with a model consisting of a thermal, Raymond-Smith (1977) plasma plus a power-law component. Since the statistics are limited in this case, we fixed the temperature and the abundance of the plasma to the mean values found in Ptak et al. (1999), namely  $kT = 0.7$  keV and  $A = 0.043 A_{\odot}$ . This fit

yielded an upper limit to the thermal flux of  $4.4 \times 10^{-13}$  ergs  $s^{-1}$   $cm^{-2}$ , or  $\sim 25\%$  of the total flux in the 0.5–2.0 keV band.

There is no evidence for significant Fe K emission at 6.4 or 6.7 keV, the expected line energies for neutral and He-like iron, although the statistics are limited. Assuming the feature to be Gaussian in shape, we find upper limits to the equivalent width of  $\sim 800$  eV for a narrow line ( $\sigma = 10$  eV) and  $\sim 1000$  eV for a broad line ( $\sigma = 100$  eV).

In order to obtain a more sensitive measure of the absorbing column, we attempted to fit the *ASCA* data simultaneously with the *ROSAT* Position Sensitive Proportional Counter (PSPC) spectrum taken by Koratkar et al. (1995). The PSPC spectrum was extracted using a circular aperture of diameter 1'.25. The combined fit yields a photon index of  $\Gamma = 1.58$  (1.51–1.66), similar to that obtained from the *ASCA* data alone, but the 0.5–2.0 keV flux is lower (by  $\sim 50\%$ ), as is the column density,  $N_H = 2.0$  ( $1.2$ – $3.3$ )  $\times 10^{20}$   $cm^{-2}$ , although the latter is statistically consistent with the *ASCA* fit. A two-component (thermal

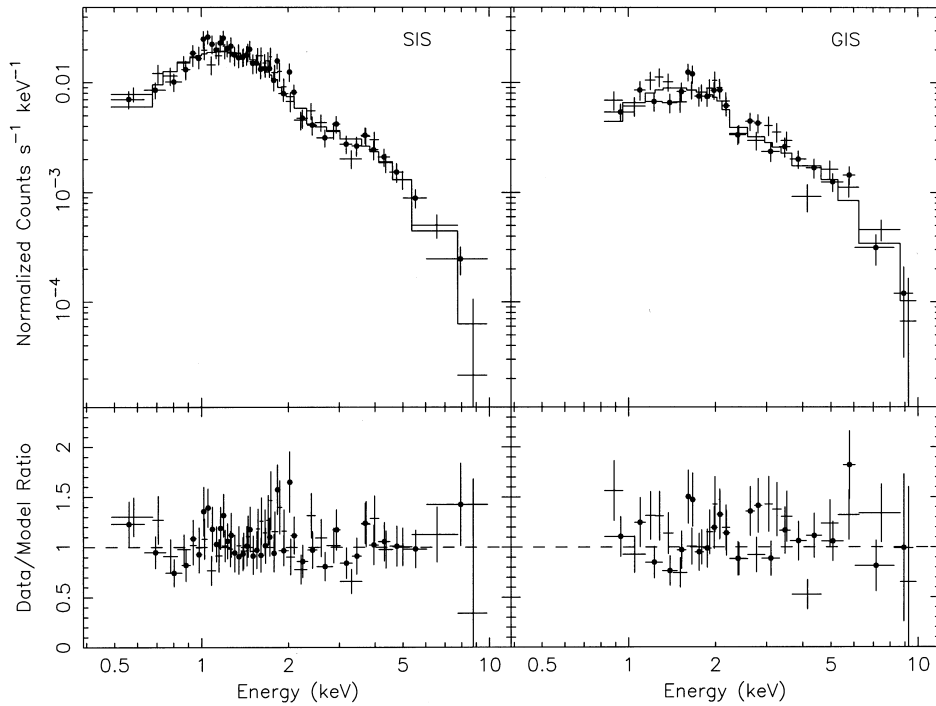


FIG. 2.—Combined *ASCA* SIS spectrum (left) and the GIS spectrum (right). The top panels show the normalized counts of the two observations, where data from the first (1997 December 17 UT) and second (1997 December 23 UT) observations are shown as unmarked and marked points, respectively. The histograms denote the best-fit absorbed power-law model. The ratio of data to model is illustrated in the bottom panels. No significant residuals are seen.

plasma plus power-law) fit once again limits the possible contribution from a thermal component to  $\lesssim 20\%$ , and the parameters of the power-law component remain essentially unchanged. Table 1 summarizes the results of the spectral fits. Note that the slope we derive for the X-ray continuum is significantly flatter than the value of  $\Gamma = 2.27 \pm 0.40$  determined by Koratkar et al. (1995) from fitting the PSPC data alone. In our joint fit we also do not find the spectral residuals at 1 keV identified by Koratkar et al. These disagreements are not surprising given the limited PSPC bandpass and the low signal-to-noise ratio of the PSPC data. Several authors have found discrepancies between *ASCA* and *ROSAT* PSPC results in the bandpass where they overlap (0.5–2.0 keV; see Iwasawa, Fabian, & Nandra 1999 and references therein), which suggests that there exists a calibration problem, most likely attributed to the PSPC, on the order of 20%–40%. Moreover, as further discussed below (§ 3.3), the nucleus of NGC 4639 clearly varies in the soft X-ray band. The results of our simulta-

neous fit should, therefore, be treated with some caution, although including the PSPC data has a very small impact on the observed hard, power-law component.

### 3.3. Variability

We searched for short-term flux variability within each of the two separate *ASCA* observations. The top panel of Figure 3 shows the light curves obtained from combining the GIS2 and GIS3 data using a bin size of 5760 s, the length of one satellite orbit, and a similar plot for the SIS0 and SIS1 data is given in the bottom panel of the figure. To access the level of variability, we performed a  $\chi^2$  test to evaluate the null hypothesis that the flux is constant. In the December 17 observation, variations are apparent at the level of  $\Delta I/I \approx 50\%$  for the SIS data; a constant model fit produces  $\chi^2_{\nu} = 2.8$  for 15 dof and therefore can be rejected at a significance level of 99.9%. The background count rate stayed constant. On the other hand, the SIS data for the second observation, taken six days later, showed no signs of

TABLE 1  
SPECTRAL FITS FOR NGC 4639

| Model                    | $N_{\text{H}}$<br>( $10^{20} \text{ cm}^{-2}$ ) | $\Gamma$         | $F(0.5\text{--}2 \text{ keV})$<br>( $\text{ergs s}^{-1} \text{ cm}^{-2}$ ) | $F(2\text{--}10 \text{ keV})$<br>( $\text{ergs s}^{-1} \text{ cm}^{-2}$ ) | $f_{\text{thermal}}$<br>(%) | $\chi^2_{\nu}/\text{dof}$ |
|--------------------------|---|------------------|--|---|-----------------------------|---------------------------|
| <i>ASCA</i>              |   |                  |  |   |                             |                           |
| Power law .....          | 7.3 (2.2–12.9)                                  | 1.68 (1.56–1.80) | $4.7 \times 10^{-13}$  | $1.1 \times 10^{-12}$   | ...                         | 0.98/491                  |
| Power law + thermal..... | 6.1 (<18.4)                                     | 1.67 (1.52–1.84) | $4.7 \times 10^{-13}$  | $1.1 \times 10^{-12}$   | <25                         | 0.98/489                  |
| <i>ASCA and ROSAT</i>    |   |                  |  |   |                             |                           |
| Power law .....          | 2.0 (1.2–3.3)                                   | 1.58 (1.51–1.66) | $2.5 \times 10^{-13}$  | $1.1 \times 10^{-12}$   | ...                         | 0.99/504                  |
| Power law + thermal..... | 1.9 (<17.9)                                     | 1.58 (1.48–1.68) | $2.5 \times 10^{-13}$  | $1.1 \times 10^{-12}$   | <20                         | 0.99/502                  |

NOTE.—The errors quoted are at the 90% level for two interesting parameters.

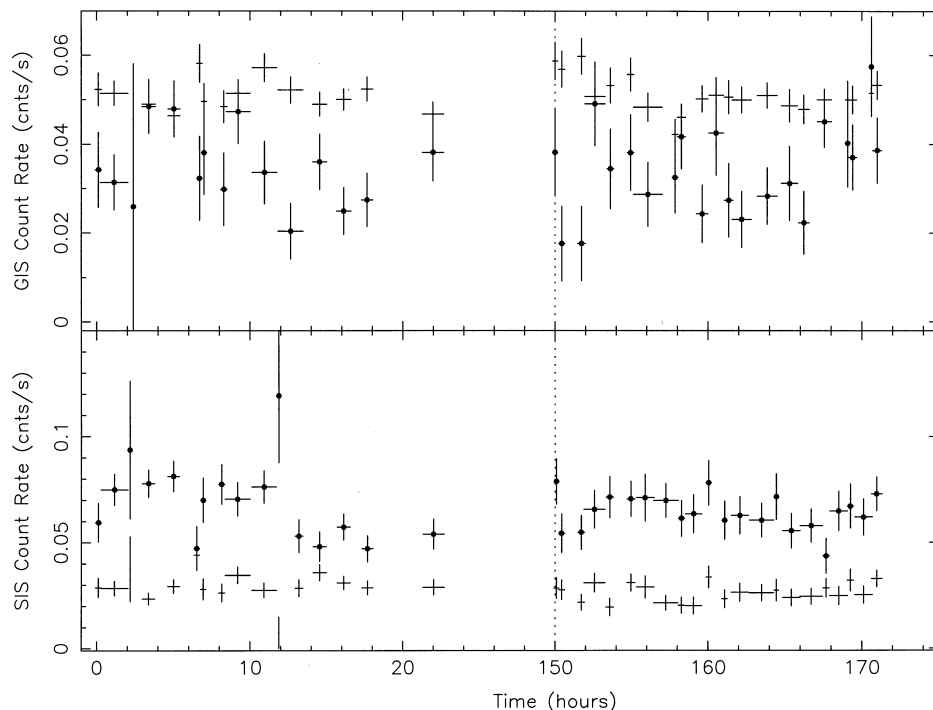


FIG. 3.—GIS (*top*) and SIS (*bottom*) light curves of NGC 4639. We have displayed the observations from both sessions on the same time axis, separated by the vertical dotted line. The data are plotted as marked points, and the background level is shown as unmarked points, binned to a bin size of 5760 s.

TABLE 2  
X-RAY FLUX HISTORY OF NGC 4639

| Detector                  | Dates       | $F(0.5-2 \text{ keV})$<br>( $\text{ergs s}^{-1} \text{ cm}^{-2}$ ) |
|---------------------------|-------------|--|
| <i>Einstein</i> IPC ..... | 1980 Jun 27 | $4.2 \times 10^{-13}$  |
| <i>ROSAT</i> HRI .....    | 1992 Jun 27 | $8.0 \times 10^{-13}$  |
|                           | 1992 Dec 12 | $4.0 \times 10^{-13}$  |
| <i>ROSAT</i> PSPC.....    | 1993 Jun 30 | $2.5 \times 10^{-13}$  |
| <i>ASCA</i> .....         | 1997 Dec 17 | $4.6 \times 10^{-13}$  |
|                           | 1997 Dec 23 | $5.0 \times 10^{-13}$  |

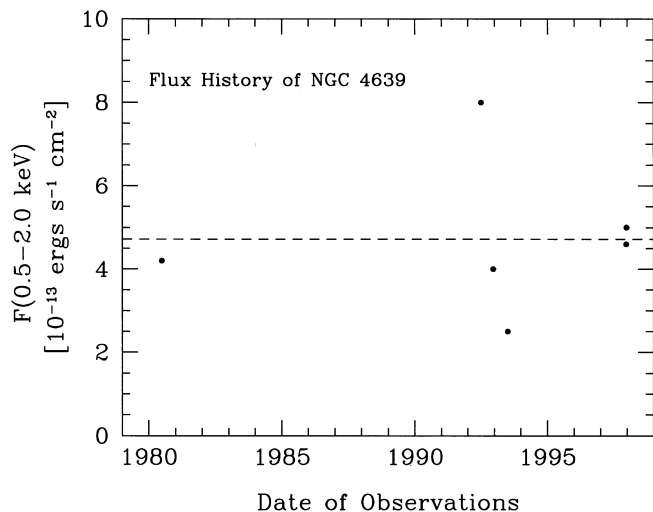


FIG. 4.—Long-term X-ray light curve of NGC 4639 over the 0.5–2.0 keV band. The horizontal dashed line denotes the average flux of all the measurements, which are listed in Table 2.

variability. A constant model fit yields  $\chi^2_\nu = 0.8$  for 21 dof. Marginal evidence of mild variability, significant at a level of  $\sim 95\%$ , may be present in both GIS observations.

We searched for variability between the two observations and found none. To assess the nature of possible X-ray variability on longer timescales, we have retrieved archival data taken with the *Einstein* IPC in 1980, as well as data acquired on three epochs in 1992 and 1993 with the *ROSAT* HRI and PSPC. For each of the *Einstein* and *ROSAT* instruments, we simulated the flux expected in the 0.5–2.0 keV band from the observed count rates and an assumed power-law model with  $\Gamma = 1.58$  and  $N_{\text{H}} = 2.0 \times 10^{20} \text{ cm}^{-2}$ , the best-fit parameters obtained from the joint *ASCA* plus *ROSAT* PSPC fit (Table 1). A summary of the flux history is presented in Table 2 and in Figure 4. The source clearly undergoes large-amplitude flux changes over timescales of several months to a year. In an interval of 6 months the two HRI pointings showed a factor of 2 variability, and the largest peak-to-peak flux change is a factor of 3.2 in 1 yr. This type of long-term X-ray variability is commonly seen in other low-luminosity AGNs (Serlemitsos et al. 1996 and references therein). The variability could be intrinsic to the source, or it could be caused by variable absorption.

## 4. DISCUSSION

### 4.1. The X-Ray Characteristics

We have established that most of the X-ray emission in NGC 4639, at both hard and soft X-ray energies, is nuclear. Although the rather coarse angular resolution of *ASCA* and *ROSAT* does not provide a stringent limit on the physical source size, the morphology does suggest that most of the

emission originates from a compact region spatially coincident with the optical center of the galaxy. Flux variability, evident in the soft and hard bands, further supports this conclusion. Most of the X-ray emission from NGC 4639, therefore, is likely to be directly associated with its weak AGN observed at optical wavelengths.

The broad resemblance of NGC 4639 to luminous Seyfert 1 nuclei extends to the spectral domain, despite the fact that its 2–10 keV luminosity is only  $\sim 8 \times 10^{40}$  ergs  $s^{-1}$ , at least a factor of  $10\text{--}10^3$  smaller than in most Seyfert galaxies conventionally studied. The spectrum of NGC 4639 from 0.5 to 10 keV, a moderately absorbed power law with a photon index of  $\Gamma \approx 1.6\text{--}1.7$ , is quite similar to the 2–10 keV spectra of more powerful AGNs (Mushotzky 1982; Turner & Pounds 1989; Nandra et al. 1997b). As in other broad-lined Seyfert nuclei, the amount of obscuration seen toward the nucleus of NGC 4639 is small. The absorbing column derived from the best-fit model is consistent with pure foreground absorption from the Galaxy and requires at most a slight excess column from the host galaxy itself. The most salient feature of the X-ray spectrum of NGC 4639—a “canonical” continuum slope—is generally seen in *ASCA* observations of other low-luminosity AGNs (see references cited in § 1). The limited photon statistics of our data, unfortunately, prevent us from making a meaningful assessment of spectral features that might be present. We cannot address, for instance, whether signatures of X-ray reprocessing by cold material, such as the fluorescent Fe K line or the Compton reflection bump, are present in the spectrum. The upper limit for the Fe K line that we derive is large enough to accommodate the range of observed line strengths.

The long-term X-ray flux history of NGC 4639 exhibits pronounced variability on timescales of months to years. With less confidence, we have argued that it also plausibly experiences mild flux changes on intervals as short as hours in the *ASCA* band. The short-term light curves of low-luminosity AGNs so far studied with *ASCA* are noteworthy for being unremarkable (Ptak et al. 1998). Among more luminous AGNs, the amplitude of variability in the hard X-ray band typically increases with decreasing X-ray luminosity (e.g., Barr & Mushotzky 1986; Lawrence & Papadakis 1993; Nandra et al. 1997a). The analysis of Nandra et al. (1997a) shows, for example, that a source such as NGC 4051, with  $L_X(2\text{--}10 \text{ keV}) \approx 7 \times 10^{41}$  ergs  $s^{-1}$  (Mihara et al. 1994, assuming  $d = 17$  Mpc), has a variability amplitude (“variance”)  $\sim 25$  times larger than, say, NGC 5548, whose  $L_X(2\text{--}10 \text{ keV}) \approx 2 \times 10^{43}$  ergs  $s^{-1}$  (Mushotzky et al. 1995, assuming  $d = 67$  Mpc). The objects in the sample of Ptak et al. (1998) are at least an order of magnitude less luminous than NGC 4051, and yet they vary much less than NGC 4051 does. Their variability behavior clearly deviates from the trend established by more luminous sources. In the case of NGC 4639, however, we have verified through simulations that variability at the level of NGC 4051 cannot be excluded by the present data.

#### 4.2. The Nature of the Central Source

What is the production mechanism of the X-ray emission in NGC 4639? Does it arise predominantly from processes similar to those in more luminous AGNs, or does it instead come from stellar sources such as X-ray binaries or starburst activity? The strength of the broad component of the hydrogen Balmer lines in luminous Seyfert 1 nuclei scales

with the observed X-ray luminosity in the 2–10 keV band (Elvis et al. 1978; Ward et al. 1988), a trend that can be interpreted as evidence that the optical emission lines are produced primarily through photoionization by the central continuum source. A similar correlation is seen in the soft X-ray band (Kriss, Canizares, & Ricker 1980), and Koratkar et al. (1995) have shown that low-luminosity sources, including NGC 4639, also obey the correlation. Terashima (1999) has recently found that broad-lined low-luminosity Seyferts and LINERs extend the  $L_{\text{H}\alpha}\text{--}L_X(2\text{--}10 \text{ keV})$  relation of Ward et al. (1988) toward the faint end. This result suggests that the hard X-ray emission in both luminosity classes share a common origin. We find that NGC 4639, too, falls on the correlation. The value of  $L_X(2\text{--}10 \text{ keV})/L_{\text{H}\alpha}$  ranges between 2.7 and 6.1 depending on the assumed extinction affecting the optical emission (see below), well within the scatter of the correlation reported by Terashima (1999).

Perhaps a more stringent test can be made by examining the shape of the ionizing continuum. Although we do not have either spectroscopic measurements in the ultraviolet (UV) or any constraints on the strength of the continuum in the extreme-ultraviolet (EUV) band, we can calculate a rudimentary two-point spectral index between 2500 Å and 2 keV,  $\alpha_{\text{ox}}$ . This quantity has an average value of 1.4 in quasars and 1.2 in luminous Seyfert 1 galaxies (Mushotzky & Wandel 1989). The central region of NGC 4639 has been observed with the Wide Field Planetary Camera 2 (WFPC2) on *HST* through the F218W filter ( $\lambda_c \approx 2150$  Å, FWHM  $\approx 356$  Å); these observations will be reported by Calvani et al. (1999). The nucleus was clearly detected as a point source with a flux density at 2500 Å of  $f_\nu = 2.0 \times 10^{-28}$  ergs  $s^{-1} \text{ cm}^{-2} \text{ Hz}^{-1}$ . The true strength of the UV emission, however, is quite uncertain because of the possible effects of dust extinction. As discussed in § 3.2, the Galaxy contributes  $E(B-V) = 0.04$  mag to the reddening, and an additional 0.03 mag, as determined from the decrement of the narrow Balmer lines, may be internal to NGC 4639. For the Galactic extinction law of Cardelli, Clayton, & Mathis (1989), dereddening by  $E(B-V) = 0.07$  mag increases the 2500 Å flux by a factor of  $\sim 1.6$ , and we find  $\alpha_{\text{ox}} = 0.95 \pm 0.01$ , where the error bars reflect the range allowed for the X-ray slope. If, on the other hand, we suppose that the value of  $N_{\text{H}}$  [ $7.3(2.2\text{--}12.9) \times 10^{20} \text{ cm}^{-2}$ ] obtained from the *ASCA* data provides a better indicator of the absorbing column affecting the UV emission, then  $E(B-V) = 0.13$  (0.04–0.22) mag, and  $\alpha_{\text{ox}} = 1.01$  (0.92–1.12). Finally, we note that it is possible that the UV continuum experiences even more severe extinction than is indicated either by the narrow-line region Balmer decrement or by the X-ray-absorbing column. The relative intensities of the broad Balmer lines, measured from the spectra published in Ho et al. (1995), suggest that the broad-line region is significantly reddened. The observed ratios of  $\text{H}\alpha:\text{H}\beta:\text{H}\gamma = 4.7:1.0:0.38$ . Whereas radiative transfer effects and collisional excitation in the broad-line region render the  $\text{H}\alpha/\text{H}\beta$  ratio an unreliable reddening indicator (see, e.g., Netzer 1975; Kwan & Krolik 1981), the intrinsic  $\text{H}\gamma/\text{H}\beta$  ratio is less susceptible to variations in physical conditions. For an intrinsic case  $B' \text{H}\gamma/\text{H}\beta = 0.47$ , the observed value indicates  $E(B-V) \approx 0.4$  mag. If this amount of reddening is appropriate for the continuum, and, furthermore, if the Galactic extinction curve is applicable, the UV emission would have to be increased by a factor of  $\sim 14$ , and  $\alpha_{\text{ox}} \approx 1.3$ . Given the many

uncertainties involved, it is obviously difficult to be definitive about the strength of the UV emission relative to the X-rays, but it appears to be roughly consistent with what is observed in more luminous Seyfert galaxies.

As an additional consistency check, the observed luminosity of the Balmer lines can be compared with that predicted from recombination theory given the ionizing luminosity, which we can compute by interpolating the spectral energy distribution between the UV and X-ray bands. For this comparison, we will use  $H\beta$  instead of  $H\alpha$  to avoid potential complications from collisional enhancement of  $H\alpha$  in the broad-line region. The total (narrow plus broad) luminosity of  $H\beta$  measured from the spectra in Ho et al. (1995) following the procedures outlined in Ho et al. (1997a, 1997b) is  $2.9 \times 10^{39}$  ergs  $s^{-1}$ , of which 94% comes from the broad component. Depending on the adopted reddening [ $E(B - V) = 0.07 - 0.4$  mag; see above], the corrected  $H\beta$  luminosity is in the range of  $(0.4 - 1.1) \times 10^{40}$  ergs  $s^{-1}$ . Case B recombination requires 8.5 Lyman continuum photons to generate an  $H\beta$  photon (Osterbrock 1989), and so the corresponding ionizing photon rate, assuming a covering factor of unity, is  $N_{\text{Lyc}}(H\beta) = (0.8 - 2.3) \times 10^{52}$   $s^{-1}$ . By contrast, the ionizing photon rate calculated by assuming an  $f_\nu \propto \nu^{-\alpha}$  spectrum with  $\alpha = \alpha_{\text{ox}}$  from the Lyman limit to 2 keV and  $\alpha = 0.68$  from 2 to 10 keV, is  $N_{\text{Lyc}} = (1.5 - 7.4) \times 10^{51}$   $s^{-1}$ , where the range once again reflects the range of probable extinction corrections. Taken at face value, this simplistic calculation suggests that the observed high-energy continuum falls short, by about a factor of 3–5, in supplying sufficient ionizing photons to sustain the observed line emission. A possible solution to this apparent discrepancy is to invoke additional extinction for the UV component. Alternatively, the shape of the ionizing continuum through the unobserved EUV region may be quite different from the simple power law that we assumed.

#### 4.3. Comparison with NGC 5033

It is instructive to compare the X-ray properties of NGC 4639 with those of NGC 5033, another nearby, low-luminosity Seyfert 1 galaxy whose optical spectrum is virtually indistinguishable from that of NGC 4639 (Ho et al. 1995, 1997b). The *ASCA* spectrum of NGC 5033, recently analyzed by Terashima, Kunieda, & Misaki (1999), is well fitted with a lightly absorbed power law with  $\Gamma = 1.7$ ,  $N_{\text{H}} = 9 \times 10^{20}$   $\text{cm}^{-2}$ , and  $L_{\text{X}}(2-10 \text{ keV}) = 2.3 \times 10^{41}$  ergs  $s^{-1}$  (for an adopted distance of 18.7 Mpc), to which is added a narrow Fe K line with rest energy 6.4 keV. With the exception of the iron line, which may have been detected in the spectrum of NGC 5033 but not in NGC 4639 because the former has significantly more counts, the X-ray spectral properties of the two objects are very similar. As in NGC 4639, moderate variability on a timescale of  $\sim 10^4$  s was also found in NGC 5033.

Ho et al. (1997b) quote a broad  $H\alpha$  luminosity of  $8.6 \times 10^{39}$  ergs  $s^{-1}$ . After adjusting this to account for reddening, estimated to be 0.4 mag from the decrement of the narrow Balmer lines, we find  $L_{\text{X}}(2-10 \text{ keV})/L_{\text{H}\alpha} = 8.8$ , a value once again in accord with the  $L_{\text{H}\alpha} - L_{\text{X}}(2-10 \text{ keV})$  relation of Terashima (1999). We can perform the same exercise we did for NGC 4639 concerning the UV emission, since NGC 5033 was also observed with *HST*/WFPC2, and it was detected as a compact UV source (Calvani et al. 1999). The observed flux density at 2500 Å is  $f_\nu = 6.3 \times 10^{-27}$  ergs

$s^{-1} \text{ cm}^{-2} \text{ Hz}^{-1}$ , which, when combined with the X-ray measurement, yields  $\alpha_{\text{ox}} = 1.2$ ; including a reddening correction of 0.4 mag increases  $\alpha_{\text{ox}}$  to 1.5. In either case, the UV–X-ray slope lies securely within the range seen in luminous AGNs. The uncorrected luminosity of the broad  $H\beta$  line, again determined from the data of Ho et al. (1995), is  $1.8 \times 10^{39}$  ergs  $s^{-1}$ . Even without extinction corrections, the Lyman continuum luminosity predicted from  $H\beta$  is only  $\sim 10\% - 40\%$  of the ionization budget estimated from interpolating the UV–X-ray continuum ( $N_{\text{Lyc}} = 1.0 \times 10^{52}$  and  $4.1 \times 10^{52}$   $s^{-1}$  for  $\alpha_{\text{ox}} = 1.2$  and 1.5, respectively), and including a reddening correction of 0.4 mag still brings the two estimates into comfortable agreement.

#### 5. SUMMARY

Low-luminosity AGNs far outnumber “classical” Seyfert nuclei and quasars, but they remain a poorly understood class of objects. Investigating sources such as NGC 4639, a relatively nearby low-luminosity Seyfert 1 galaxy, may provide valuable clues for understanding the AGN phenomenon in general and for exploring the connections between the “active” and “normal” galaxy populations. The X-ray properties of NGC 4639 were previously discussed by Koratkar et al. (1995) based on *ROSAT* observations. The present study uses new *ASCA* data to extend the analysis into hard X-ray energies as well as UV measurements obtained with *HST*, and we reconsider the overall X-ray properties of this source in light of these new observations.

The nucleus of NGC 4639 was detected as a compact hard X-ray source. The *ASCA* spectrum can be modeled as a slightly absorbed ( $N_{\text{H}} = 7.3 \times 10^{20}$   $\text{cm}^{-2}$ ) power law with a photon index of  $\Gamma \approx 1.7$  and a luminosity of  $L_{\text{X}}(2-10 \text{ keV}) = 8.3 \times 10^{40}$  ergs  $s^{-1}$ . Inspection of archival *Einstein* and *ROSAT* data reveals that the nucleus varies in the soft X-ray band on timescales of months to years, and there is marginal evidence of more rapid ( $\sim 10^4$  s) variability within the *ASCA* data sets. If the variability is intrinsic to the source and not due to variable absorption, it would rule out the possibility that the power-law component arises from scattering, as was found to be the case for NGC 3147 (Ptak et al. 1996). No significant contribution from a thermal plasma with a temperature of 0.7 keV, a trait common in other low-luminosity AGNs, was detected at soft X-ray energies.

NGC 4639, despite being 1–3 orders of magnitude less luminous in the X-rays than most Seyfert galaxies previously studied, exhibits X-ray characteristics that are quite similar to those of more powerful sources. Both the strength of its broad  $H\alpha$  emission line, measured from ground-based spectra, and its UV emission, measured from *HST* images, scale with the X-ray luminosity in roughly the same manner as do luminous AGNs. There is a discrepancy of a factor of a few between the ionizing luminosity estimated from the UV–X-ray continuum and that inferred from the luminosity of the Balmer emission lines, but in view of the uncertainties inherent in the assumptions of our calculations, this disagreement is probably not serious. Recent studies have noted key aspects in which low-luminosity AGNs differ from high-luminosity AGNs. Ptak et al. (1998) find, for example, that the rapid variability behavior of low-luminosity objects clearly departs from the trend set by luminous sources. The variability amplitude of NGC 4639, on the other hand, appears not to be anomalous. It is also

noteworthy that the UV–X-ray spectral energy distribution of NGC 4639, at least as crudely described by the  $\alpha_{\text{ox}}$  parameter, does not appear to be noticeably different from that of more luminous sources. This is in stark contrast to the set of low-luminosity objects studied by Ho (1999), most of which have X-ray luminosities comparable to that of NGC 4639, whose spectral energy distributions tend to be much more prominent in the X-rays compared with the UV band. NGC 4639—along with NGC 5033, a source that is similar to NGC 4639 in many ways and that we also briefly discuss—serves as a useful reminder that some low-

luminosity AGNs appear to be simple extensions of high-luminosity objects.

L. C. H. acknowledges partial support from NASA grants NAG5-3556 and AR-07527.02-96A, the latter awarded by the Space Telescope Science Institute (operated by AURA, Inc., under NASA contract NAS5-26555). Jane Turner, the referee, offered helpful suggestions for improving the paper. We thank Humberto Calvani for supplying the *HST* UV flux measurements for NGC 4639 and NGC 5033.

## REFERENCES

- Barr, P., & Mushotzky, R. F. 1986, *Nature*, 320, 421  
 Bohlin, R. C., Savage, B. D., & Drake, J. K. 1978, *ApJ*, 224, 132  
 Calvani, H., et al. 1999, in preparation  
 Cardelli, J. A., Clayton, G. C., & Mathis, J. S. 1989, *ApJ*, 345, 245  
 de Vaucouleurs, G., de Vaucouleurs, A., Corwin, H. G., Jr., Buta, R. J., Paturel, G., & Fouqué, R. 1991, *Third Reference Catalogue of Bright Galaxies* (New York: Springer)  
 Elvis, M., Maccacaro, T., Wilson, A. S., Ward, M. J., Penston, M. V., Fosbury, R. A. E., & Perola, G. C. 1978, *MNRAS*, 183, 129  
 Filippenko, A. V., & Sargent, W. L. W. 1985, *ApJS*, 57, 503  
 ———. 1986, in *Structure and Evolution of Active Galactic Nuclei*, ed. G. Giuricin et al. (Dordrecht: Reidel), 21  
 Gaskell, C. M., & Ferland, G. J. 1984, *PASP*, 96, 393  
 Ho, L. C. 1999, *ApJ*, 516, 672  
 Ho, L. C., Filippenko, A. V., & Sargent, W. L. W. 1995, *ApJS*, 98, 477  
 ———. 1997a, *ApJS*, 112, 315  
 Ho, L. C., Filippenko, A. V., Sargent, W. L. W., & Peng, C. Y. 1997b, *ApJS*, 112, 391  
 Ishisaki, Y., et al. 1996, *PASJ*, 48, 237  
 Iwasawa, K., Fabian, A. C., & Nandra, K. 1999, *MNRAS*, 307, 611  
 Iyomoto, N., Makishima, K., Matsushita, K., Fukazawa, Y., Tashiro, M., & Ohashi, T. 1998, *ApJ*, 503, 168  
 Koratkar, A. P., Deustua, S., Heckman, T. M., Filippenko, A. V., Ho, L. C., & Rao, M. 1995, *ApJ*, 440, 132  
 Kriss, G. A., Canizares, C. R., & Ricker, G. R. 1980, *ApJ*, 242, 492  
 Kwan, J., & Krolik, J. H. 1981, *ApJ*, 250, 478  
 Lawrence, A., & Papadakis, I. 1993, *ApJ*, 414, L85  
 Mihara, T., Matsuoka, M., Mushotzky, R. F., Kunieda, H., Otani, C., Miyamoto, S., & Yamauchi, M. 1994, *PASJ*, 46, L137  
 Murphy, E. M., Lockman, F. J., Laor, A., & Elvis, M. 1996, *ApJS*, 105, 369  
 Mushotzky, R. F. 1982, *ApJ*, 256, 92  
 Mushotzky, R. F., Fabian, A. C., Iwasawa, K., Kunieda, H., Matsuoka, M., Nandra, K., & Tanaka, Y. 1995, *MNRAS*, 272, L9  
 Mushotzky, R. F., & Wandel, A. 1989, *ApJ*, 339, 674  
 Nandra, K., George, I. M., Mushotzky, R. F., Turner, T. J., & Yaqoob, T. 1997a, *ApJ*, 476, 70  
 ———. 1997b, *ApJ*, 477, 602  
 Netzer, H. 1975, *MNRAS*, 171, 395  
 Nicholson, K. L., Reichert, G. A., Mason, K. O., Puchnarewicz, E. M., Ho, L. C., Shields, J. C., & Filippenko, A. V. 1998, *MNRAS*, 300, 893  
 Osterbrock, D. E. 1981, *ApJ*, 249, 462  
 ———. 1989, *Astrophysics of Gaseous Nebulae and Active Galactic Nuclei* (Mill Valley: University Science Books)  
 Ptak, A., Serlemitsos, P. J., Yaqoob, T., & Mushotzky, R. 1999, *ApJS*, 120, 179  
 Ptak, A., Yaqoob, T., Mushotzky, R., Serlemitsos, P., & Griffiths, R. 1998, *ApJ*, 501, L37  
 Ptak, A., Yaqoob, T., Serlemitsos, P. J., Kunieda, H., & Terashima, Y. 1996, *ApJ*, 459, 542  
 Raymond, J. C., & Smith, B. W. 1977, *ApJS*, 35, 419  
 Sandage, A., Saha, A., Tammann, G. A., Labhardt, L., Panagia, N., & Macchetto, F. D. 1996, *ApJ*, 460, L15  
 Sandage, A. R., & Tammann, G. A. 1981, *A Revised Shapley-Ames Catalog of Bright Galaxies* (Washington, DC: Carnegie Inst. Washington)  
 Serlemitsos, P., Ptak, A., & Yaqoob, T. 1996, in *ASP Conf. Ser. 103, The Physics of LINERs*, ed. M. Eracleous, A. Koratkar, C. Leatherer, & L. Ho (San Francisco: ASP), 70  
 Tanaka, Y., Inoue, H., & Holt, S. S. 1994, *PASJ*, 46, L37  
 Terashima, Y. 1999, *Adv. Space Res.*, 23(5-6), 851  
 Terashima, Y., Kunieda, H., & Misaki, K. 1999, *PASJ*, 51, 277  
 Turner, T. J., & Pounds, K. A. 1989, *MNRAS*, 240, 833  
 Ward, M. J., Done, C., Fabian, A. C., Tennant, A. F., & Shafer, R. A. 1988, *ApJ*, 324, 767  
 Weedman, D. W. 1976, *ApJ*, 208, 30